Scripta Materialia 211 (2022) 114508

Contents lists available at ScienceDirect

Scripta Materialia

journal homepage: www.elsevier.com/locate/scriptamat

Accessing the role of Joule heating on densification during flash sintering of YSZ

Subhadip Bhandari[a,b], Tarini Prasad Mishra[b,*], Olivier Guillon[b], Devinder Yadav[a,*], Martin Bram[b]

[a] Department of Metallurgical and Materials Engineering, Indian Institute of Technology Patna, Bihta, Patna, Bihar 801106, India
[b] Forschungszentrum Jülich GmbH, Institute of Energy and Climate Research, Materials Synthesis and Processing (IEK-1), 52428, Jülich, Germany

ARTICLE INFO

Article history:
Received 18 November 2021
Revised 15 December 2021
Accepted 6 January 2022
Available online 11 January 2022

Keywords:
Flash sintering
Electric field assisted sintering
Joule heat
Defects
Yttria stabilized Zirconia

ABSTRACT

Flash sintering is a novel electric field and current assisted sintering technique which densify ceramics at moderate furnace temperature and in short time (few seconds) as compared to the conventional sintering techniques. The onset of flash encompasses three unique characteristics, (i) non-linear rise in conductivity, (ii) luminescence and (iii) rapid densification. the mechanism behind the flash phenomena is not fully understood yet. The present work experimentally demonstrated that the densification in flash sintering is primarily dominated by Joule heating. Herein, we distinguished the onset of flash and the degree of densification of cubic zirconia in sintering atmospheres with different oxygen partial pressures. In this study, we demonstrate that the flash onset temperature and densification are independently influenced by the sintering atmosphere during flash sintering. Furthermore, the extent of densification is not directly influenced by the current density rather, by the power dissipated in the sample.

Main body

Flash sintering is a novel field-assisted sintering technique that has emerged as an energy-efficient method to densify ceramics in few seconds at relatively lower furnace temperatures, as compared to the conventional sintering processes. Since its discovery in 2010 by Cologna et al. [1], wide range of ceramic materials including ionic conductors, proton conductors, electronic conductors, semiconductors and insulators have been flash sintered [2–4]. Flash sintering process exhibits the following characteristics: (i) non-linear rise in the conductivity (ii) luminescence and (iii) ultra-fast densification. The underlying mechanisms for the flash sintering process remains debated in the literature. However, several theories have been proposed based on Joule heating [5–7], electrochemical reduction [8–10], local melting at particle contacts [11], and nucleation of Frenkel defects (avalanche of defects) [12–14], to explain the ultra-rapid densification.

In a typical flash sintering experiment, a constant electric field is applied across the sample which is accompanied by a non-linear rise in the conductivity, monitored by an increase in current. This is termed as the onset of flash, which causes a surge in power dissipation in the sample [15]. The electrical power to the sample is then switched from voltage-control to current-control in order to prevent electrical/thermal runaway. This transition is accompanied by rapid densification to near full density, typically within seconds. Previous studies showed that the applied electric field controls the furnace temperature at which flash onset occurs, while the extent of densification is controlled by the set current density [16,17]. The flash onset temperature can be reduced by increasing the applied electric field. However, Debye temperature of a material is currently seen as a lower-bound temperature for the onset of flash [12,18,19]. Previous studies show that lower oxygen partial pressure environment decreases the flash onset temperature [8,20–22]. It is worth mentioning here that a decrease in the flash onset temperature by changing the atmosphere will be energetically advantageous, however, the detailed effect of sintering atmosphere on the densification behavior still needs to be accessed.

Zhang et al. [20] reported that the onset of flash can be achieved at a significantly lowered temperature in low $P(O_2)$ atmosphere in ZnO. However, the sample flash sintered in low $P(O_2)$ atmosphere showed less densification as compared to in air [20]. Similarly, Liu et al. [21] and Mishra et al. [8] also reported the lowering of onset temperature in low $P(O_2)$ atmosphere for 3YSZ and gadolinia doped ceria (GDC), respectively. In a recent study, Wang et al. [22] reported significant reduction in the flash onset temperature from 648 °C in air to 239 °C in an inert (Ar) atmosphere for TiO_2. The decrease in the flash onset temperature has been primarily attributed to the enhanced conductivity of the sample in low

* Corresponding authors.
E-mail addresses: t.mishra@fz-juelich.de (T.P. Mishra), devinder@iitp.ac.in (D. Yadav).

https://doi.org/10.1016/j.scriptamat.2022.114508
1359-6462/

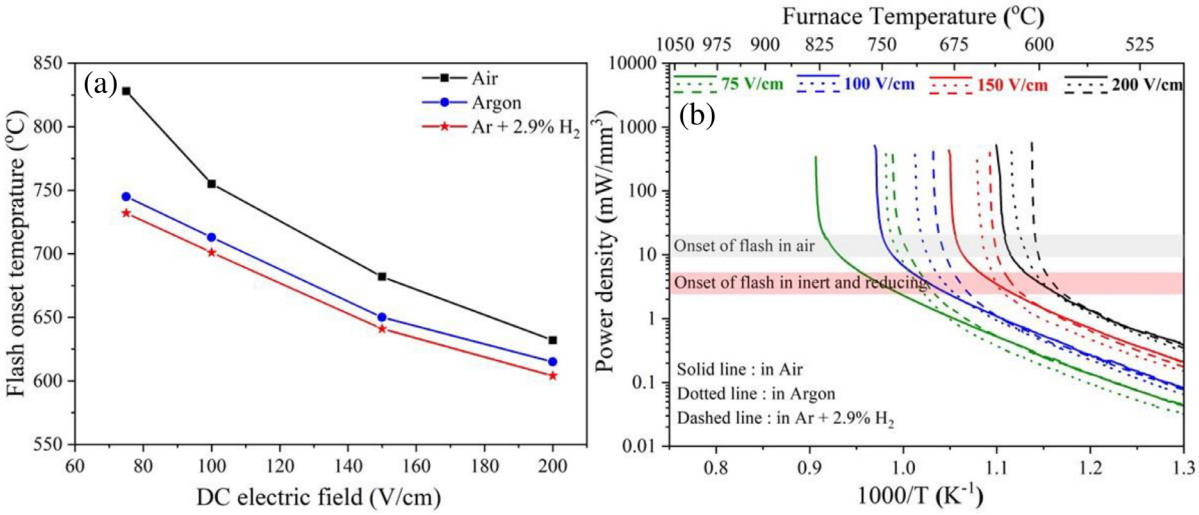

Fig. 1. (a) Flash onset temperature for 8YSZ as a function of applied electric field in air, Argon and Ar+2.9% H_2 (b) Arrhenius plots for power density in air, Argon and Ar+2.9% H_2 atmosphere.

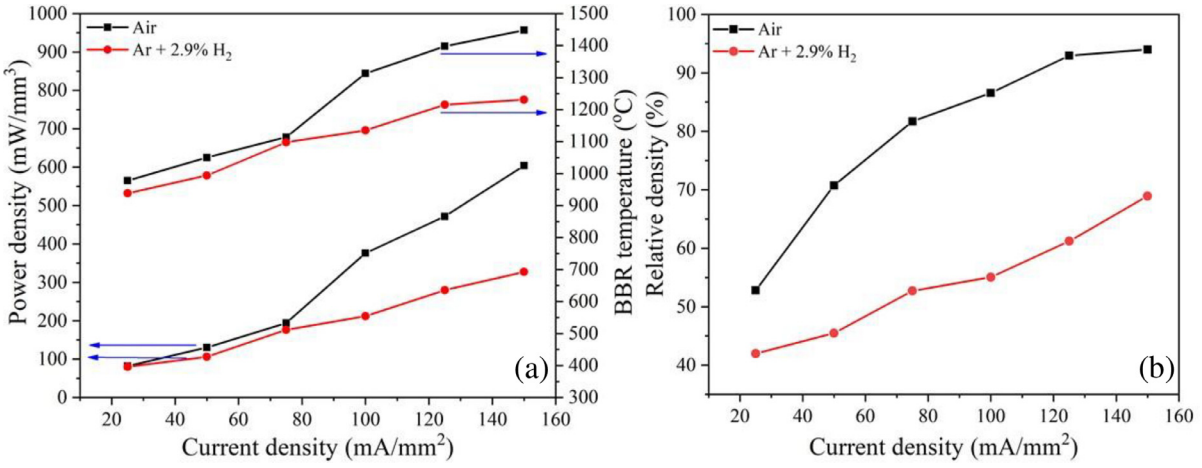

Fig 2. (a) Variation of the power dissipation and BBR temperature in stage III with the current density (b) Influence of current density on the relative density.

oxygen partial pressure environments. Although extensive research has been carried out on zirconia-based materials, a comprehensive discussion on the influence of atmosphere on the onset of flash, densification and the resultant microstructure is still missing.

In the present work, effect of atmosphere on the flash onset temperature and densification behavior of 8 mol.% yttria stabilized zirconia (8YSZ) was studied. We have experimentally distinguished the two characteristics of flash sintering i.e., onset of flash and densification, which are generally discussed as concurrent events. It is demonstrated here that the onset of flash does not support densification. Furthermore, a novel *in-situ* atmosphere-controlled flash experiment was carried out to experimentally demonstrate that the degree of densification directly depends on the power dissipation in the sample. The microstructure of the sintered samples was evaluated with respect to the electrode polarity.

Powders of 8YSZ (Tosoh corporation, Japan) with average particle size of 155 nm were uniaxially pressed into dog-bone shape, having length, breadth and thickness of 15 mm, 3.5 mm and 2.3–2.6 mm, respectively. The samples were pre-sintered at 900 °C for 1 h. The relative density of the green samples was ~45% of the theoretical value. The microstructure of the pre-sintered samples shows no grain growth but only neck formations between primary particle contacts (supplementary Fig. S1). The pre-sintered samples were loaded in a vertical tubular furnace with a pair of platinum wires which were connected to a DC power supply (Sorensen DLM 300-2).

Flash sintering experiments were performed in two different modes, (i) Constant heating rate (CHR), where electric field was applied across the sample followed by heating the furnace at a constant rate of 10 °C/min. Three different atmospheres were used with regard to the oxygen partial pressure: air, Ar and Ar+2.9% H_2. The oxygen content was maintained at around 10^{-18} ppm and 10^{-4} ppm in Ar+2.9% H_2 and Ar, respectively. Experiments were performed at four different electric fields: 75, 100, 150 and 200 V/cm at a pre-set current density limit of 75 mA/mm^2. (ii) Isothermal experiments were carried out at a furnace temperature of 830 °C and 775 °C in air and Ar+2.9% H_2, respectively at an applied electric field of 100 V/cm. The samples were flash sintered at current densities varying from 25 to 150 mA/mm^2 (in steps of 25). The furnace was held at isothermal temperature for 15 min before switching on the power supply to ensure uniform temperature across the sample. The samples were held in the state of flash (stage III) for 30 s. The current and voltage were measured using a digital multimeter (Keithley2000, Keithley Instruments, Cleveland, USA). The sample temperature in the stage III of flash was estimated using the black-body radiation model [23].

The ear sections of the sintered specimen were removed and only the gage section was analysed for all the characterization. The

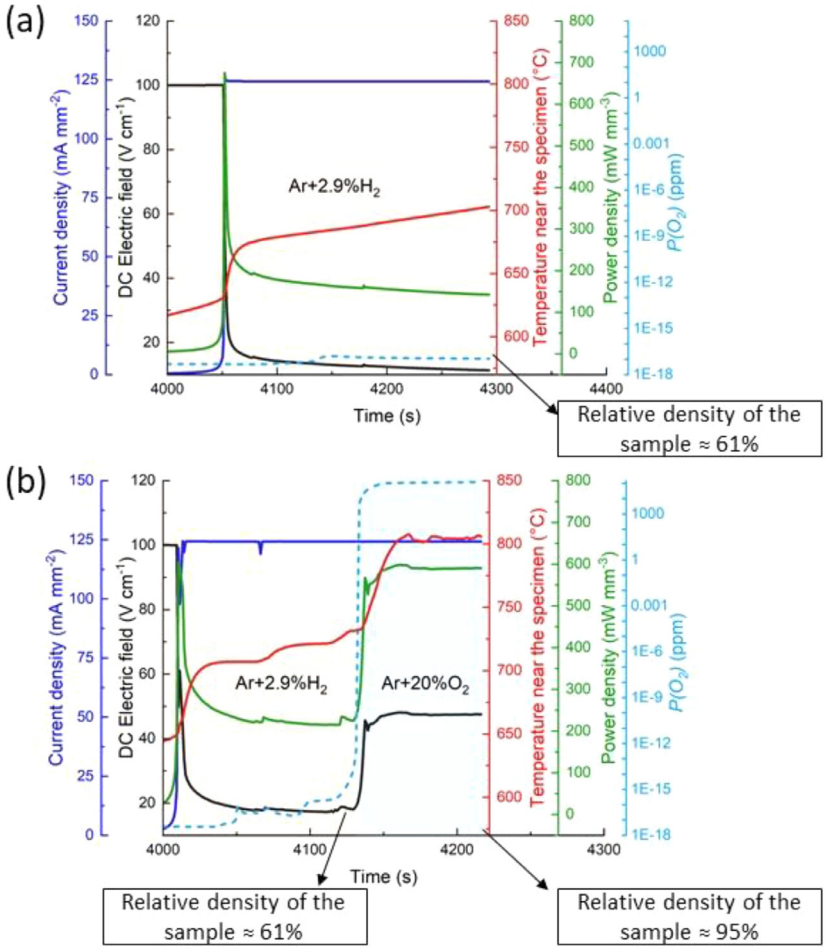

Fig 3. CHR Flash sintering experiment in (a) under Ar+2.9% H_2 atmosphere and (b) *in-situ* re-oxidation: initially Ar+2.9% H_2 and then oxidizing atmosphere.

density of the sintered specimen was measured by Archimedes principle using water as a medium. The samples sintered in air were polished and thermally etched for 1 h at a temperature 170 °C less than the black-body radiation temperature. The microstructural analysis was performed in a Zeiss Ultra55 FEG-SEM. Grain size was measured by linear intercept method using the graphical user interface Linecut, running on MATLAB program [24]. The flash onset is characterized by a non-linear rise in the electrical conductivity of the specimen. This is the point where the sample temperature rises above the furnace temperature. To find out the exact temperature at which the non-linearity begins, the tangent method was employed on the first derivative of the power density [12]. The method is described in the Supplementary file (Fig. S2).

Fig. 1(a) shows the flash onset temperature against applied electric field for 8YSZ samples, flash sintered in three different atmospheres. The flash onset temperature decreased as the applied electric field increased, which is in agreement with the previous findings [25,26]. Furthermore, at a particular electric field, the onset temperature decreased as the partial pressure of oxygen decreased. For example, at an applied electric field of 100 V/cm, the flash onset temperature decreased from 755 °C in air to 713 °C in an inert (Ar) atmosphere ($P(O_2)$ $\sim 10^{-4}$ ppm) and further decreased to 701 °C in reducing atmosphere of Ar+2.9% H_2 ($P(O_2)$ $\sim 10^{-18}$ ppm). The decrease in the onset temperature was more prominent at lower electric fields. The Arrhenius plots used for estimating the power dissipation at the onset of flash, where the transition from linear to non-linear increase of conductivity depends on the atmosphere, is shown in Fig. 1(b). The flash onset is reported to occur within a narrow range of power density (5–30 mW/mm^3) for a variety of materials [27]. Power dissipation at the onset of flash was higher in air when compared to the inert and reducing atmospheres. This result signal towards the relationship between the conductivity of the sample and the onset of flash, which might be helpful in understanding the reduction in the flash onset temperature of 8YSZ with decreasing $P(O_2)$, as explained below.

Yttria is the most commonly used dopant for stabilizing the cubic phase of zirconia at room temperature and it also increase the ionic conductivity. Substitution of Zr^{4+} with Y^{3+}, leads to the generation of oxygen vacancies to maintain charge neutrality. It is denoted by Kroger-Vink notation:

$$ZrO_2 \xrightarrow{Y_2O_3} 2Y'_{Zr} + 3O_o^x + V_o^{\cdot\cdot} \quad (1)$$

In low oxygen partial pressure environment, the oxide tends to give up oxygen, it will do so by creating oxygen vacancies in the lattice. Hence, the creation of vacant oxygen sites leads to a change in the cation to anion ratio, which is known as oxygen non-stoichiometry. Apart from generation of oxygen vacancies, free electrons are also generated during this process to maintain the charge neutrality. This is denoted by the following Kroger-Vink notation [28]:

$$O_o^x \rightarrow \frac{1}{2}O_2 + V_o^{\cdot\cdot} + 2e^- \quad (2)$$

Thus, reduction in the oxygen partial pressure results in the increase in the concentration of oxygen vacancies and associated free electrons, which enhances the overall conductivity of the speci-

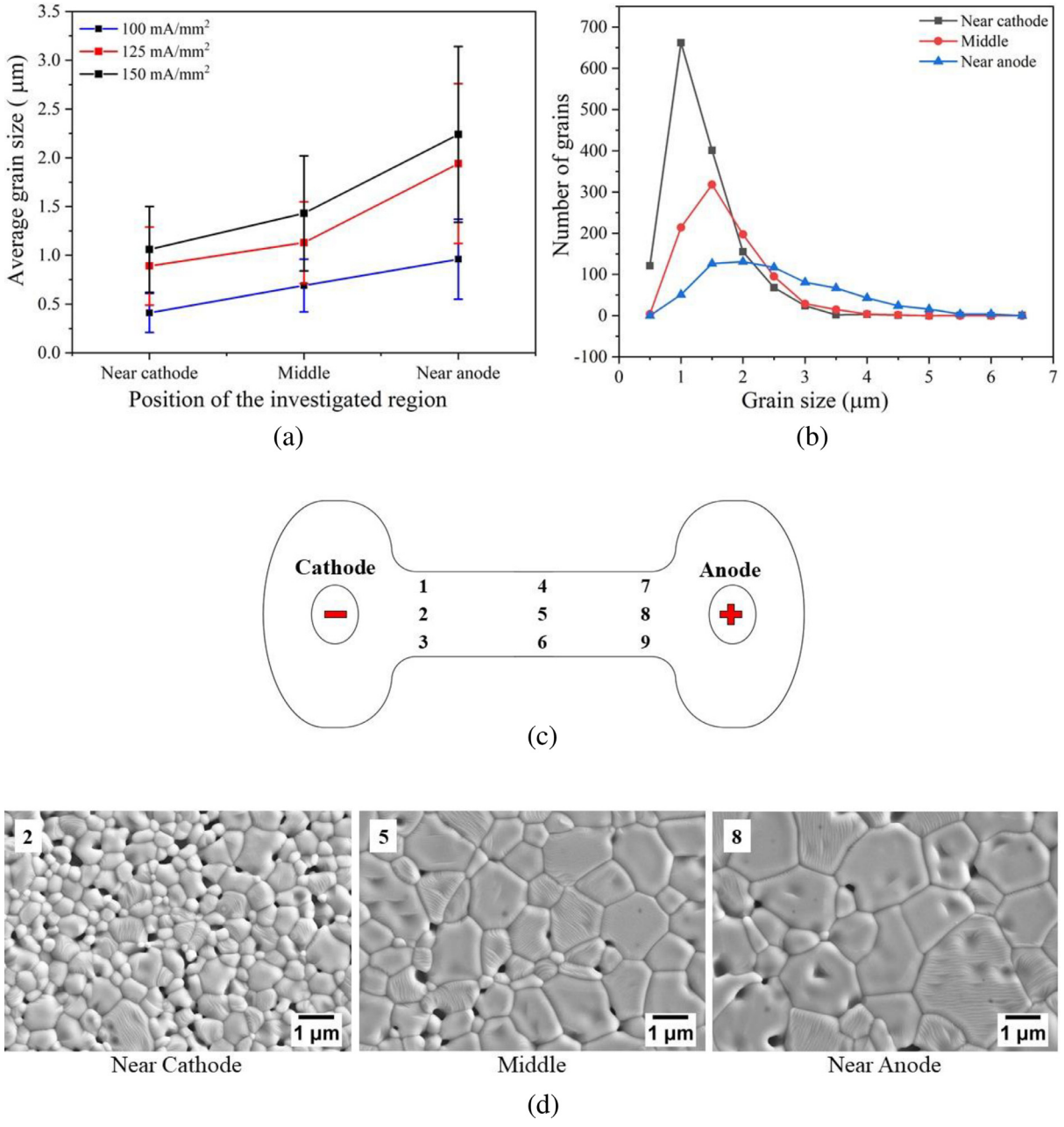

Fig 4. (a) Variation of the grain size with the position of the investigated region, (b) Grain size distribution of the sample, (c) Schematic representation of the investigated positions in the gage section for microstructural analysis (d) Microstructure of the 8YSZ sample at three different positions (2, 5 and 8 in Fig.3(c)) flash sintered at a current density of 150 mA/mm^2 in air.

men. As a result of this increased conductivity, the flash onset temperature is lowered in oxygen-deprived environments, which promote the onset of flash at lower temperature.

The enhanced conductivity in inert/reducing atmosphere resulted in the reduction of the resistance against the flow of current, consequently, the power dissipation (I^2R) decreases. This can be clearly seen in Fig. 1(b) where the power dissipation at the onset of flash in inert/reducing atmosphere (marked in light red) is lower when compared to air (marked in light gray). Recent study by Biesuz et al. [29] also reported a decrease in the power density at the flash onset of the YSZ/Al_2O_3 composites by increasing the volume percentage of conductive phase (i.e., YSZ) in the composite. The result confirms Joule heating as the primary origin of the onset of flash. Nevertheless, the athermal effects of the applied electric field cannot be ignored completely [8,30].

The flash sintered samples in inert and reducing atmosphere showed blackening at the negative electrode side, which appeared to propagate towards the positive electrode side. On the contrary, the samples that were flash sintered in air did not show any noticeable blackening. Blackening of the sample and the associated electrochemical reduction of the sample is described in the Supplementary file (Fig. S3).

Isothermal flash sintering experiments were performed to understand the influence of the pre-set current density limit on the densification process in different atmospheres. Fig. 2(a) shows the average power density and the estimated sample temperature (by black-body radiation model) in stage III, at various current densities. The average power density increased with increase in the maximum current density. Likewise, the sample temperature increased as the current density increased. Nevertheless, the average

power density and the estimated sample temperature were lower for the samples flash sintered in reducing atmosphere, when compared to the samples flash sintered in air.

Fig. 2(b) depicts the influence of current density on the extent of densification. The relative density of the flash sintered specimen increased with increasing current density in both the atmospheres. However, the extent of densification in air was higher when compared to the reducing atmosphere. The sample flash sintered in air achieved a maximum density of ~95%, whereas in the case of Ar+2.9% H_2 it was ~68%, at a current density of 150 mA/mm^2.

The relative density of the flash sintered samples can be directly correlated to the power dissipation. The higher the power dissipated, the higher is the sample temperature. Hence, the sample sintered in air could be densified to a larger extent as compared to the reducing atmosphere. This is an important finding, which can separate the entanglement between the two important characteristics of the flash sintering process that is, onset of the flash and densification. Reducing atmosphere enhance the conductivity of the samples, which cause the flash onset to occur at a lower temperature. However, the enhanced conductivity results in lower resistance of the sample and lower power dissipation, which cause lower densification of the sample. This suggests that the densification is directly influenced by the heat generated in the sample due to Joule heating.

To access the role of Joule heating on the densification of the sample during flash sintering, two unique flash sintering experiments were carried out. Fig. 3 shows an overview of the electrical and thermal data of the CHR flash sintering experiment. It is to be noted that the data only around the flash event is shown in the images. The complete cycles of these CHR experiments can be found in the supplementary figures (Fig. S4).

The first CHR flash sintering experiment was carried out completely in Ar+2.9% H_2 atmosphere. The sample was held after the onset of flash for approximately 210 s. The current density was limited to 125 mA/mm^2. The density of the flash sintered sample was measured to be approximately 61%. The second CHR flash experiment was performed with similar processing parameters and starting in Ar+2.9% H_2 atmosphere, however, the oxygen partial pressure was changed in a controlled manner, in stage III. It can be seen from the plot that the power dissipation was almost same as in the first experiment. After 130 s, the atmosphere of the furnace was switched to ambient air. The partial pressure of oxygen was monitored for the complete cycle and the change in $P(O_2)$ is evident from Fig. 3(b). It appears that the resistance of the sample changed when the $P(O_2)$ was increased. The increased $P(O_2)$ results in the re-oxidation of the sample which now decrease the sample conductivity as per the reverse reaction mentioned in equation (2). Therefore, the net power dissipation in the sample increased. The increased power dissipation resulted in increased sample temperature by Joule heating, which was also confirmed by the temperature increase recorded by the thermocouple, placed very near the sample. The flash sintered sample from the re-oxidation experiment showed a densification of around 95%.

As the densification of the flashed sample in reducing atmosphere was less, only the microstructure of the samples flash sintered in air was investigated. The grain size analysis for the samples flash sintered in air at current densities of 100, 125 and 150 mA/mm^2 is shown in Fig. 4(a). However, there are contrary reports on the microstructural homogeneity across the flash sintered samples with enhanced grain growth either at the anode or the cathode side [31–35]. Hence, the microstructure of the samples was analysed since any heterogeneity will cause change of the properties The grain size distribution for the sample flash sintered at a current density of 150 mA/mm^2 is graphically plotted in Fig. 4(b). The grain size was calculated at various locations along the gage length, marked 1–9 in Fig. 4(c).

Fig. 4(a) shows the microstructural asymmetry due to the polarity induced effects (DC electric field). Quantitatively, the grains on the anode side were almost twice the size of grains on the cathode side. The inhomogeneity of the grain size at different electrodes can be explained by the electrochemically induced temperature gradient in the sample as explained previously for GDC material [35]. Furthermore, the temperature gradient was confirmed by melting of the platinum electrodes at the anode side at higher current densities.

In summary, we demonstrate here that the flash onset temperature and densification are independently influenced by the sintering atmosphere during flash sintering. The sintering atmosphere has the potential to influence of the concentrations of defects which in turn affects the onset of the flash. The extent of densification depends on the power dissipated in the sample. The microstructural asymmetry in the sintered microstructure is attributed to the electrical polarity induced electrochemical reduction.

Declaration of Competing Interest

None.

Acknowledgments

The financial support from German Academic Exchange Service (DAAD), under the program “Combined Study and Practice Stays for Engineers from Developing Countries (KOSPIE) with Indian IITs, 2020” (ID: 57525292) is highly acknowledged. The authors also acknowledge funding from the German Science Foundation (DFG), under priority program “Fields Matter” (SPP 1959) under the Grant No. BR 3418/1-2.

Supplementary materials

Supplementary material associated with this article can be found, in the online version, at doi:10.1016/j.scriptamat.2022.114508.

References

[1] M. Cologna, B. Rashkova, R. Raj, . Am. Ceram. Soc. 93 (2010) 3556–3559.
[2] M. Biesuz, V.M. Sglavo, J. Eur. Ceram. Soc. 39 (2019) 115–143.
[3] M. Yu, S. Grasso, R. Mckinnon, T. Saunders, M.J. Reece, Adv. Appl. Ceram. 116 (2017) 24–60.
[4] C.E.J. Dancer, Mater. Res. Express 3 (2016) 102001.
[5] R.I. Todd, E. Zapata-Solvas, R.S. Bonilla, T. Sneddon, P.R. Wilshaw, J. Eur. Ceram. Soc. 35 (2015) 1865–1877.
[6] Y. Zhang, J.I. Jung, J. Luo, Acta Mater. 94 (2015) 87–100.
[7] R. Baraki, S. Schwarz, O. Guillon, J. Am. Ceram. Soc. 95 (1) (2012) 75–78.
[8] T.P. Mishra, R.R.I. Neto, G. Speranza, A. Quaranta, V.M. Sglavo, R. Raj, O. Guillon, M. Bram, M. Biesuz, Scr. Mater. 179 (2020) 55–60.
[9] S. Jo, R. Raj, Scr. Mater. 174 (2020) 29–32.
[10] C.A. Grimley, A.L.G. Prette, E.C. Dickey, Acta Mater. 174 (2019) 271–278.
[11] R. Chaim, Materials 9 (2016) 280 (Basel).
[12] D. Yadav, R. Raj, J. Am. Ceram. Soc. 100 (2017) 5374–5378.
[13] K.S. Naik, V.M. Sglavo, R. Raj, J. Eur. Ceram. Soc. 34 (2014) 4063–4067.
[14] C. Schmerbauch, J. Gonzalez- Julian, R. Röder, C. Ronning, O. Guillon, J. Am. Ceram. Soc. 97 (6) (2014) 1728–1735.
[15] R. Raj, J. Am. Ceram. Soc. 99 (2016) 3226–3232.
[16] J.S.C. Francis, R. Raj, J. Am. Ceram. Soc. 96 (2013) 2754–2758.
[17] T.P. Mishra, C. Lenser, R. Raj, O. Guillon, M. Bram, J. Am. Ceram. Soc. 104 (2021) 4316–4328.
[18] T.P. Mishra, V. Avila, R.R.I. Neto, M. Bram, O. Guillon, R. Raj, Scr. Mater. 170 (2019) 81–84.
[19] M. Jongmanns, R. Raj, D.E. Wolf, New J. Phys. 20 (2018) 093013.
[20] Y. Zhang, J. Luo, Scr. Mater. 106 (2015) 26–29.
[21] D. Liu, Y. Cao, J. Liu, Y. Gao, Y. Wang, J. Eur. Ceram. Soc. 38 (2018) 817–820.
[22] Q. Wang, C.S. Watts, C.E. Athanasiou, Z. Dai, M. Hu, B.W. Sheldon, N.P. Padture, Scr. Mater. 199 (2021) 113894.
[23] R. Raj, J. Eur. Ceram. Soc. 32 (10) (2012) 2293–2301.
[24] Meister S., grain and particle analysis with line intersection method - File Exchange - MATLAB Central [Internet]. Mathworks.com. 2012 [cited 08 January 2022]. Available from: https://www.mathworks.com/matlabcentral/fileexchange/35203-grain-and-particle-analysis-with-lineintersection-method.

[25] M. Cologna, A.L. Prette, R. Raj, J.f Am. Ceram. Soc. 94 (2) (2011) 316–319.
[26] J.A. Downs, V.M. Sglavo, J. Am. Ceram. Soc. 96 (5) (2013) 1342–1344.
[27] D. Yadav, R. Raj, Scr. Mater. 134 (2017) 123–127.
[28] J. Janek, C. Korte, Solid State Ion. 116 (1999) 181–195.
[29] M. Biesuz, A. Ometto, V. Tyrpekl, M. Vilémová, V.M. Sglavo, Scr. Mater. 201 (2021) 113984.
[30] O. Guillon, R.A. De Souza, T.P. Mishra, W. Rheinheimer, MRS Bull. 46 (2021) 52–58.
[31] W. Qin, H. Majidi, J. Yun, K. van Benthem, J. Am. Ceram. Soc. 99 (2016) 2253–2259.
[32] W. Rheinheimer, X.L. Phuah, H. Wang, F. Lemke, M.J. Hoffmann, H. Wang, Acta Mater. 165 (2019) 398–408.
[33] Y.Y. Zhang, J.I. Jung, J. Luo, Acta Mater. 94 (2015) 87–100.
[34] M. Biesuz, V.M. Sglavo, Scr Mater. 150 (2018) 82–86.
[35] T.P. Mishra, C. Lenser, R. Raj, O. Guillon, M. Bram, J. Am. Ceram. Soc. 104 (2021) 4316–4328.